





Orientation-dependent stabilization of MgCr_2O_4 spinel thin filmsFangdi Wen ^{*}, Xiaoran Liu ^{*}, Mikhail Kareev, Tsung-Chi Wu, Michael Terilli, and Jak Chakhalian
*Department of Physics and Astronomy, Rutgers University, Piscataway, New Jersey 08854, USA*Padraic Shafer ^{*} and Elke Arenholz[†]
Advanced Light Source, Lawrence Berkeley National Laboratory, Berkeley, California 94720, USA (Received 18 August 2020; accepted 9 October 2020; published 28 October 2020)

AB_2O_4 normal spinels with a magnetic B site can host a variety of magnetic and orbital frustrations leading to spin-liquid phases and field-induced phase transitions. Here, we report the epitaxial growth of (111)-oriented MgCr_2O_4 thin films. By characterizing the structural and electronic properties of films grown along the (001) and (111) directions, the influence of growth orientation has been studied. Despite distinctly different growth modes observed during deposition, the comprehensive characterization reveals no measurable disorder in the cation distribution nor multivalency issue for Cr ions in either orientation. Contrary to a naive expectation, the (111) stabilized films exhibit a smoother surface and a higher degree of crystallinity than (001)-oriented films. The preference in growth orientation is explained within the framework of heteroepitaxial stabilization in connection to a significantly lower (111) surface energy. These findings open broad opportunities in the fabrication of two-dimensional kagome-triangular heterostructures with emergent magnetic behavior inaccessible in bulk crystals.

DOI: [10.1103/PhysRevB.102.165426](https://doi.org/10.1103/PhysRevB.102.165426)**I. INTRODUCTION**

Geometrically frustrated magnets have received considerable attention, and great effort has been put forward to identify and characterize frustration-induced phenomena [1–4]. In two dimensions (2D), many antiferromagnetic materials with a triangular lattice motif can harbor frustrated interactions, making them excellent candidates for exotic behavior including quantized magnetization plateaus [5], charge frustration in mixed-valence spinels [6,7], order by disorder [8], valence-bond ordering [9,10], moleculelike spin clusters [11,12], and potentially spin-liquid states [4,13–17]. Despite a plethora of theoretical predictions, only a few highly frustrated candidates have been investigated in detail so far [3,4,14,17]. For instance, in three dimensions (3D), corner-sharing tetrahedral pyrochlores $\text{A}_2\text{B}_2\text{O}_7$ with spins coupled either ferromagnetically or antiferromagnetically have been proposed to host numerous interesting phenomena stemming from macroscopic ground-state degeneracy [1,18–22]. In close analogy to pyrochlores, spinels (AB_2O_4) represent another materials family that exhibits a corner-sharing tetrahedron network, with the B site ions forming a pyrochlore sublattice and A site ions organized into a moderately frustrated diamond sublattice [23–26]. Based on this observation, it is unsurprising that spinels also demonstrate many unusual low-temperature magnetic phenomena linked to the massive ground-state degeneracy such as spin-glass, spin-ice, and spin-liquid states [18,27–32].

In this paper, we specifically focus on MgCr_2O_4 (MCO). MCO is a normal spinel that crystallizes into the cubic $Fd\bar{3}m$ space group with $a = 8.33 \text{ \AA}$ [33,34]. In this spinel, the Cr^{3+} ($3d^3$) ions are octahedrally coordinated by oxygen ions resulting in an $S = 3/2$ high-spin state under the cubic crystal field. Due to the direct overlap between t_{2g} orbitals, the antiferromagnetic exchange is dominant between nearest-neighbor Cr^{3+} ions leading to the high Curie-Weiss temperature $\Theta_{\text{CW}} = -400 \text{ K}$ [34,35]. On the other hand, the corner-sharing tetrahedra sublattice of Cr^{3+} ions remains paramagnetic down to the transition temperature $T_N = 12.5 \text{ K}$, yielding a moderate value of the frustration parameter $f = |\Theta_{\text{CW}}|/T_N \sim 32$. At T_N , the system undergoes a magnetostructural phase transition driven by the strong spin-lattice coupling [33,34,36–38]. Several neutron scattering experiments have elucidated the underlying frustrated behavior leading to the discovery of a highly frustrated spin texture and “proximate” spin liquid due to the short-range exchange interaction [39–42].

In parallel to those developments, in pursuit of enhanced and tunable exchange interactions accompanied by strongly elevated magnetic frustration, a geometrical lattice engineering approach based on the synthesis of thin films of spinels along (111) becomes an increasingly popular direction [30–32,43–45]. To illustrate this approach, we note that along the (111) direction, the Cr sublattice consists of alternating kagome and triangular atomic planes formed by magnetically active Cr^{3+} ions [see Fig. 1(a)]. Thus the expectation is that by growing MCO(111) thin films, one can lower the dimensionality and shift the energy balance to activate stronger exchange interactions to potentially reach new magnetic states with frustrated behavior unattainable in the bulk. Despite the intriguing proposals linked to the (111) geometry, to our best

^{*}fangdi.wen@rutgers.edu[†]Present address: Cornell High Energy Synchrotron Source, Cornell University, Ithaca, NY 14853.

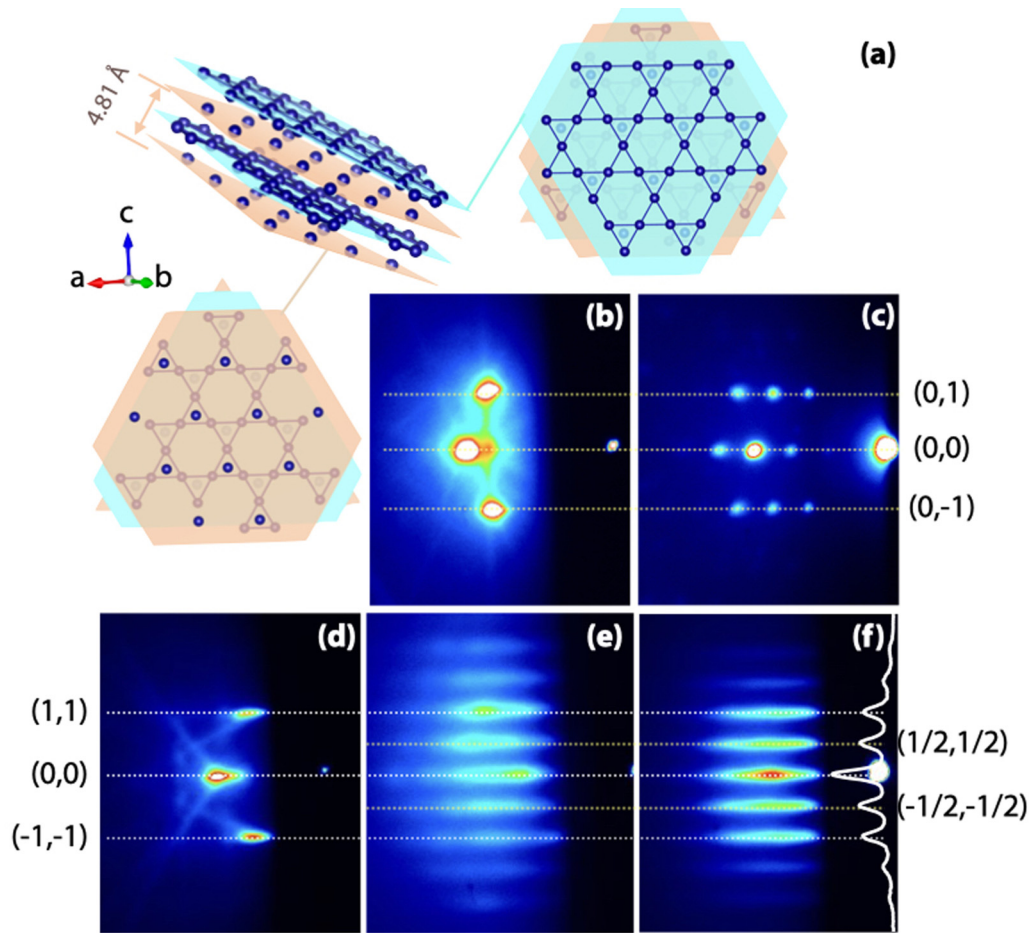


FIG. 1. (a) Schematic showing Cr atoms in MCO when viewed along (111) planes. (b) RHEED pattern from the (001) surface of MAO before growth. (c) RHEED pattern of MCO(001) grown on MAO(001). (d) RHEED image of the AlO (0001) substrate. (e) RHEED pattern of MCO(111) grown on MAO(111). (f) RHEED pattern of MCO(111) grown on AlO(0001). The inset curve is a vertical line profile. All samples are grown at 550 °C and 2 mTorr of pure oxygen.

knowledge, the growth of MCO thin films still needs to be demonstrated. It is also interesting to note that in the bulk a wide variety of methods have been applied to synthesize MCO crystals, including ceramic synthesis, coprecipitation, the sol-gel method, combustion, the hydrothermal method, zone melting, and cocrystallization [46,47]. However, to date, the size of MCO crystals is still limited, which hinders the application of powerful experimental probes [48–53].

In this paper, we describe the growth of MCO(111) and MCO(001) thin films created by way of epitaxial stabilization using pulsed laser deposition (PLD) with *in situ* reflection high-energy electron diffraction (RHEED). All the samples are characterized by x-ray reflectivity (XRR) and x-ray diffraction (XRD) using the Empyrean platform by Malvern Panalytical. X-ray photoelectron spectroscopy (XPS) was performed in a $K\alpha$ x-ray photoelectron spectrometer (Thermo Fisher Scientific). Synchrotron-based x-ray absorption spectroscopy (XAS) was carried out on beamline 4.0.2 at the Advanced Light Source, Lawrence Berkeley National Laboratory. Based on a thorough analysis and contrary to the initial expectation, the results demonstrate that MCO growth on a (111) surface is preferentially stabilized over the conventional (001) growth. This result was attributed to

the significant difference in the orientation-dependent Gibbs energy during the initial phase of nucleation and growth. The successfully stabilized high-quality MCO(111) thin films expand the boundary of the materials phase space beyond the bulk and potentially enable different magnetic states with frustrated behavior.

II. EXPERIMENT

A series of MCO films have been prepared on (100)- and (111)-oriented surfaces. All samples were grown by pulsed laser deposition with the same laser power of ~ 2 J/cm², pulse rate of 4 Hz, and monitored by *in situ* RHEED. During the deposition, the best growth condition occurs for the substrate temperature of 550 °C and 2 mTorr oxygen background pressure. After the growth, all films were annealed at the growth condition for 10 min, and then cooled down to room temperature at 15 °C/min under the same oxygen pressure. Particularly, to create (111)-oriented films, we focused on two different substrates. One is the MgAl₂O₄ spinel (MAO), which has the same structural morphology and a lattice mismatch $\epsilon = (a_{\text{MAO}} - a_{\text{MCO}})/a_{\text{MCO}} \sim -2.9\%$ (compressive strain). As for the second choice, we selected α -Al₂O₃ (AlO),

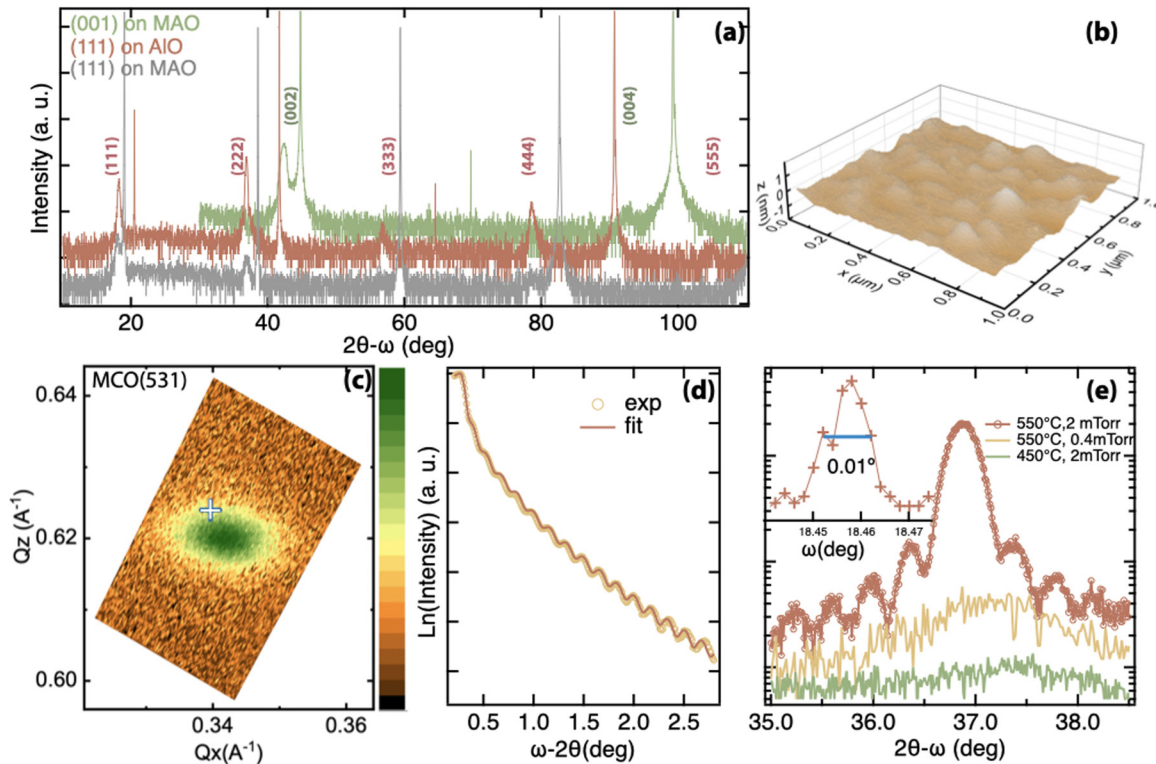


FIG. 2. (a) Full-range XRD scans of MCO(001) film grown on MAO, MCO(111) film grown on AIO (orange), and MCO(111) film grown on MAO under the same deposition condition. (b) An atomic force microscopy image of MCO(111) grown on the AIO substrate. The averaged rms roughness in the $1 \mu\text{m} \times 1 \mu\text{m}$ area is 171 pm. (c) RSM of MCO (531) film peak measured on 80-nm MCO (111) film. (d) XRR of the MCO(111) film, whose XRD is shown in (a), along with the fitting result. From the fitting, the film thickness is estimated to be around 23 nm. (e) Zoomed-in XRD scan around (222) peak measured on films grown under various conditions. The inset is the ω scan of MCO (111) (550°C , 2 mTorr) around the (222) film peak; the estimated FWHM is 0.01° .

whose oxygen sublattice is in close registry with the MCO oxygen sublattice. Here, we note the in-plane averaged O-O distance of AIO is 2.75 \AA while the O-O distance on the (111) surface of MCO is 2.95 \AA , resulting in the *continuity of the anion sublattice* across the film/substrate interface albeit with a larger compressive strain of $\sim -6.8\%$.

In order to grow MCO (001), we used MAO (001) as a substrate. As shown in Figs. 1(b) and 1(c), after the deposition of MCO, sharp streaks in the RHEED pattern were observed with the vertical spacing matching the substrate (0,1) and (0, -1) reflections. This observation is typical for the films crystallized in the Stranski-Krastanov growth mode. However, after switching to the (111) surface of an otherwise identical MAO substrate, sharp RHEED peaks rapidly turn into diffuse streaks along the (1, -1) axis, as illustrated in Fig. 1(e). This observation implies that after changing the substrate orientation from (111) to (001), the growth mode is switched to the Frank-van der Merve (3D island) mode. Surprisingly, despite the more substantial disparity in the crystal structure and larger strain, the AIO substrate serves as a better template for growing MCO(111). Figures 1(d) and 1(f) compare the RHEED patterns of the AIO (0001) substrate with the MCO film. As clearly seen, the RHEED pattern of the substrate peaks (-1, -1) and (1,1) matches well with the (-1, -1) and (1,1) RHEED reflections of the film. Since the in-plane lattice constant of MCO is twice that of AIO, an extra pair

of strong reflections appears almost immediately after the initial deposition [marked by $(\pm 1/2, \pm 1/2)$ in Fig. 1(c)]. A direct comparison to Fig. 1(e) reveals much smoother streaked features with an overall lower background observed after deposition on the AIO substrate, confirming the Frank-van der Merve growth mode. These findings signify the critical importance of matching the anion network over the magnitude of strain. One can speculate that a possible reason for the observed island growth on the MAO (111) substrate is that the polar MAO (111) surface is compensated for the polar discontinuity with ordered oxygen vacancies leading to the reconstructed $(6\sqrt{3} \times 6\sqrt{3})$ areas. As a result, the charge-compensated surface will consist of a juxtaposition of the original oxygen-terminated MAO (111) domains disrupted by oxygen-deficient areas that impede the MCO crystallization [54,55].

To further investigate the effect of oxygen pressure and temperature on the growth, a detailed analysis of the crystallinity of a series of samples was carried out by XRD and XRR. Figure 2(a) shows that no additional chemical phases were observed in any of the films regardless of the orientation or the growth mode. Moreover, for similar thicknesses, the MCO(111) on the MAO substrate demonstrates much weaker film peaks than the film grown on AIO, further confirming that the AIO substrate with an oxygen-matched sublattice indeed markedly improves the crystallinity of the MCO films.

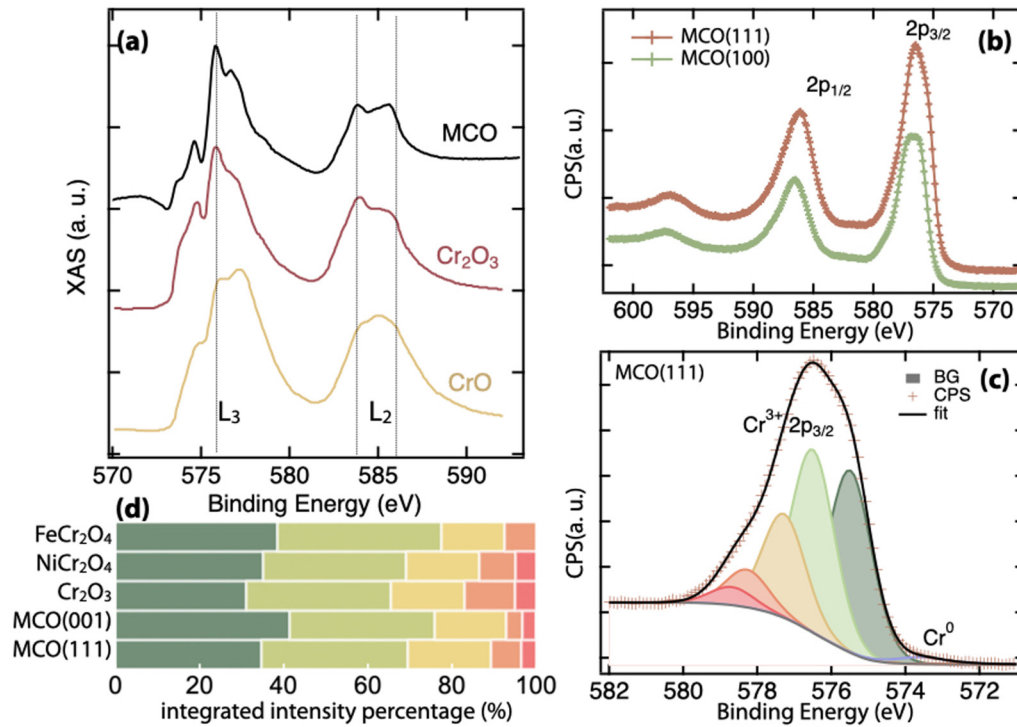


FIG. 3. (a) XAS of MCO (111) measured at room temperature in comparison to XAS of Cr₂O₃ and CrO. Cr₂O₃ and CrO XAS were adapted from Ref. [56]. (b) Experimental full-range XPS result for MCO (111) and MCO(001). (c) Zoomed-in Cr 2p_{3/2} XPS with fitting. The five main peaks are the fine structure of Cr³⁺ as a result of multiplet splitting, which is standard for chromium (III) oxides. The other small peak is Cr⁰ due to the surface charging effect. The χ^2 of this fit is 0.399. (d) The integrated intensity of the five peaks shown in (c) in percentage, observed in other closely related systems [57,58] compared to the fitting result of MCO(111) and MCO(100).

In what follows, we focus on the atomic force microscopy (AFM), XRR, and reciprocal space map (RSM) results conducted on the MCO grown on AlO. The analysis of an XRD scan shown in Fig. 2(a) yields the out-of-plane lattice constant of 4.87 Å which under the assumption of a tetragonal distortion results in $\sim 0.6\%$ in-plane elongation which is in accord with the tensile in-plane strain. XRR data [Fig. 2(d)] confirm the presence of a very homogeneous film texture with a slow exponential intensity roll-off due to the surface roughness $\sigma = 436 \pm 3$ pm. As illustrated in Fig. 2(b), this low value of roughness was corroborated by the atomic force microscopy result (rms roughness of ~ 171 pm). Besides, the ω scan measured around the (222) film Bragg reflection shows a very sharp single peak with a full width at half maximum (FWHM) of $\sim 0.01^\circ$ [see the inset of Fig. 2(e)], further affirming the excellent film crystallinity. To verify the strain state, we measured the reciprocal space map (RSM) around the off-symmetry (531) peak on a thicker sample of 80 nm [see Fig. 2(c)]. By comparing the observed film peak position to the calculated bulk value marked by a white cross, it is clear that the film is compressed in plane and stretched along the c axis (i.e., tetragonally distorted). The estimated in-plane strain value is -0.5% , which is in a good agreement with the value obtained from the 2θ - ω XRD data (-0.6%). Overall, these results confirm that imposed strain is robust and is only partially relaxed in the thick MCO(111) film. In sharp contrast to the (111)-oriented growth, for the MCO(100), the out-of-plane lattice constant remained practically unchanged after deposition, which is consistent

with the Stranski-Krastanov growth mode initially revealed by *in situ* RHEED.

In addition to the growth of MCO under the ideal growth condition, other growth conditions have been thoroughly explored. Here, we briefly discuss the film crystallinity dependence on substrate, temperature, and pressure on (111)-oriented MCO films. Figure 2(e) shows the MCO (222) Bragg reflection for three representative samples grown under different deposition conditions: S1: 550 °C, 2 mTorr; S2: 550 °C, 0.4 mTorr; and S3: 450 °C, 2 mTorr. By zooming in to the (222) reflection, it is clear that there is a distinct oxygen pressure boundary at about 1 mTorr and a temperature threshold at ~ 500 °C. Below these boundaries, the out-of-plane lattice constant estimated from the peak position becomes closer to the bulk value of 4.83 Å for S2 and 4.81 Å for S3. Besides that, the changes in temperature and oxygen pressure do not affect MCO's growth mode along (001). Finally, all films become amorphous when grown under vacuum below 10^{-4} Torr, as evidenced by the absence of film peaks in XRD.

Next, we turn our attention to the electronic structure of the films. The electronic state and elemental composition were analyzed for MCO films grown in different orientations. First, since the x-ray absorption (XAS) can fingerprint the electronic configuration and spin state of MCO, we investigated the films by XAS at the Cr L_{2,3} edge at room temperature. Figure 3(a) shows the absorption data taken on the MCO films in comparison to the well-known Cr²⁺ and Cr³⁺ reference compounds. As immediately seen, apart from some minor intensity variations, the spectral features of MCO(111) largely

mimic those of Cr_2O_3 (Cr^{3+}) and are distinct from the Cr^{2+} spectral line shape. Additional evidence for expected Cr^{3+} was obtained from the XPS measurement showing the presence of a clear $2p$ doublet, and a pair of shakeup satellite peaks following the doublet at a higher binding energy. Next, we fitted the chromium $2p_{3/2}$ peak following the Cr_2O_3 (Cr^{3+}) references [57,58]. As shown in Fig. 3(c), by comparing the MCO(111) peak distribution to the reference Cr^{3+} compounds CrO , Cr_2O_3 , NiCr_2O_4 , and FeCr_2O_4 , we conclude that the peak positions and their relative intensity indeed closely follow the XPS results for the Cr^{3+} systems with an analogous oxygen coordination. Interestingly, despite the 3D growth of MCO(100), the overall XPS core-state positions and the fine structure closely resemble the other chromium Cr^{3+} compounds as well as MCO (111). Specifically, no extra peaks, such as Cr IV, V, or VI, have been detected by XPS.

III. DISCUSSION

During our search for an ideal growth condition for MCO (001), other substrates (e.g., MgO) and growth conditions (O_2 pressure varied from 10^{-5} to 0.1 Torr, the temperature varied from 450 to 750 °C) have been explored. Despite these efforts, the MCO(001) films form in one of two ways: Either they develop 3D growth with high roughness, or exhibit poor microcrystallinity though with a correct charge and chemical state. In sharp contrast, MCO(111) films can be grown in a layer-by-layer way, as seen in RHEED and XRD. Thus it is natural to ask the following: Why is MCO(111) easier to stabilize than MCO(001)?

To address this question, we have made a Gibbs free-energy comparison according to the model of heteroepitaxial stabilization [59]. The energy difference ΔE after the deposition can be primarily attributed to three parts: $\Delta E = \Delta G_v + \Delta G_{\text{strain}} + \Delta G_{\text{surface}}$, where $\Delta G_{\text{strain}} \propto \epsilon^2$ (ϵ is the lattice mismatch), and ΔG_v is the specific volume Gibbs energy, which depends only on the initial and final chemical composition. For MCO, ΔG_v is approximately $-49\,200$ (± 400) J at the growth temperature [60]. The negative value of ΔE means that the film growth is energetically favored. Now we can compare MCO (001) and MCO (111) growth based on the energy argument; first, experimentally we have determined that MCO (111) stabilizes easier than MCO (001), i.e., $\Delta E^{111} < \Delta E^{001}$. Second, the XPS result shows that the end composition for both orientations is a pure MCO spinel without secondary chemical phases, therefore $\Delta G_v^{111} = \Delta G_v^{001}$. Next, for the same substrate but under different orientations, we observed better growth on the MAO (111) substrate than

on MAO (001). Last but not least, we take into account the fact that AlO, as a substrate, has a larger lattice mismatch ϵ than MAO (i.e., $\Delta G_{\text{strain}}^{111} > \Delta G_{\text{strain}}^{001}$). Finally, taking the above three points into consideration, one can conclude that indeed $\Delta G_{\text{surface}}^{111} < \Delta G_{\text{surface}}^{001}$.

This result is further corroborated by the data on spinel MAO and other spinel ferrites, showing that the (111) surface has a significantly lower surface energy than the (001) surface [61]. More specifically, the specific surface energy can be written as $\nu = \lambda h^2 / \pi^2 d$, where λ is the elastic modulus normal to the plane under consideration, d is the periodicity, and h is the interlayer spacing. For different orientations, $\lambda_{(001)} = C_{11}$ and $\lambda_{(111)} = (1/3)(C_{11} + 2C_{12} + 4C_{44})$. By adapting the elastic constants $C_{11} = 315.53$ GPa, $C_{12} = 206.73$ GPa, $C_{44} = 90.10$ GPa [62,63], one can estimate the surface energy of MCO along the (001) and (111) direction to be ~ 1664 and 276 erg/cm², respectively. This large disparity in the surface energy strongly influences the initial nucleation process lending strong support to the hypothesis that MCO should preferentially stabilize on the (111) surface, which overall agrees well with the data.

In conclusion, we have grown epitaxially stabilized MCO(111) films on the Al_2O_3 substrate. The MCO films deposited along the (111) direction show excellent layer-by-layer growth while MCO films growth along (001) show a Stranski-Krastanov (islandlike) growth mode, albeit with correct morphology and chemical composition. The samples' high crystallinity was evaluated by XRR and XRD, and the chemical composition and electronic structure confirmed by XPS and XAS. The high-quality growth along (111) is explained in the framework of heteroepitaxial stabilization and attributed primarily to the markedly lower surface energy of MCO(111) compared to (001). The presented methodology of growth of (111)-oriented spinel thin films based on the symmetry matching of anyon sublattices across the interface opens up rich research opportunities to probe spin dynamics in novel frustrated 2D systems.

ACKNOWLEDGMENTS

F.W. was supported by the Claud Lovelace Graduate Fellowship and Department of Energy under Grant No. DE-SC0012375. X.L., M.K., T.-C.W., M.T., and J.C. acknowledged the support by the Gordon and Betty Moore Foundation EPiQS Initiative through Grant No. GBMF4534. This research used resources of the Advanced Light Source, which is a DOE Office of Science User Facility under Contract No. DE-AC02-05CH11231.

- [1] L. Balents, Spin liquids in frustrated magnets, *Nature (London)* **464**, 199 (2010).
- [2] J. S. Wen, S. L. Yu, S. Y. Li, W. Q. Yu, and J. X. Li, Experimental identification of quantum spin liquids, *npj Quantum Mater.* **4**, 9 (2019).
- [3] Y. Zhou, K. Kanoda, and T. K. Ng, Quantum spin liquid states, *Rev. Mod. Phys.* **89**, 025003 (2017).
- [4] M. R. Norman, Colloquium: Herbertsmithite and the search for the quantum spin liquid, *Rev. Mod. Phys.* **88**, 041002 (2016).

- [5] S. Y. Zhu, L. Y. Kong, L. Cao, H. Chen, M. Papaj, S. X. Du, Y. Q. Xing, W. Y. Liu, D. F. Wang, C. M. Shen, F. Z. Yang, J. Schneeloch, R. D. Zhong, G. D. Gu, L. Fu, Y. Y. Zhang, H. Ding, and H. J. Gao, Nearly quantized conductance plateau of vortex zero mode in an iron-based superconductor, *Science* **367**, 189 (2020).
- [6] R. Koborinai, S. E. Dissanayake, M. Reehuis, M. Matsuda, T. Kajita, H. Kuwahara, S. H. Lee, and T. Katsufuji, Orbital Glass State of the Nearly Metallic Spinel Cobalt Vanadate, *Phys. Rev. Lett.* **116**, 037201 (2016).

- [7] A. Uehara, H. Shinaoka, and Y. Motome, Charge-spin-orbital fluctuations in mixed valence spinels: Comparative study of AlV_2O_4 and LiV_2O_4 , *Phys. Rev. B* **92**, 195150 (2015).
- [8] A. Avella, A. M. Oles, and P. Horsch, Defect-Induced Orbital Polarization and Collapse of Orbital Order in Doped Vanadium Perovskites, *Phys. Rev. Lett.* **122**, 127206 (2019).
- [9] Y. Shimizu, H. Akimoto, H. Tsujii, A. Tajima, and R. Kato, Mott Transition in a Valence-Bond Solid Insulator with a Triangular Lattice, *Phys. Rev. Lett.* **99**, 256403 (2007).
- [10] M. Tamura, A. Nakao, and R. Kato, Frustration-induced valence-bond ordering in a new quantum triangular antiferromagnet based on $[\text{Pd}(\text{dmit})_2]$, *J. Phys. Soc. Jpn.* **75**, 093701 (2006).
- [11] C. Schroder, H. Nojiri, J. Schnack, P. Hage, M. Luban, and P. Kogerler, Competing Spin Phases in Geometrically Frustrated Magnetic Molecules, *Phys. Rev. Lett.* **94**, 017205 (2005).
- [12] M. L. Baker, G. A. Timco, S. Piligkos, J. S. Mathieson, H. Mutka, F. Tuna, P. Kozłowski, M. Antkowiak, T. Guidi, T. Gupta, H. Rath, R. J. Woolfson, G. Kamieniarz, R. G. Pritchard, H. Weihe, L. Cronin, G. Rajaraman, D. Collison, E. J. L. McInnes, and R. E. P. Winpenny, A classification of spin frustration in molecular magnets from a physical study of large odd-numbered-metal, odd electron rings, *Proc. Natl. Acad. Sci. U.S.A.* **109**, 19113 (2012).
- [13] V. O. Garlea, L. D. Sanjewa, M. A. McGuire, C. D. Batista, A. M. Samarakoon, D. Graf, B. Winn, F. Ye, C. Hoffmann, and J. W. Kolis, Exotic Magnetic Field-Induced Spin-Superstructures in a Mixed Honeycomb-Triangular Lattice System, *Phys. Rev. X* **9**, 011038 (2019).
- [14] L. Savary and L. Balents, Quantum spin liquids: A review, *Rep. Prog. Phys.* **80**, 016502 (2016).
- [15] M. Hermanns, I. Kimchi, and J. Knolle, Physics of the Kitaev model: Fractionalization, dynamic correlations, and material connections, *Annu. Rev. Condens. Matter Phys.* **9**, 17 (2018).
- [16] H. Takagi, T. Takayama, G. Jackeli, G. Khaliullin, and S. E. Nagler, Concept and realization of Kitaev quantum spin liquids, *Nat. Rev. Phys.* **1**, 264 (2019).
- [17] C. Broholm, R. J. Cava, S. A. Kivelson, D. G. Nocera, M. R. Norman, and T. Senthil, Quantum spin liquids, *Science* **367**, eaay0668 (2020).
- [18] J. S. Gardner, M. J. P. Gingras, and J. E. Greedan, Magnetic pyrochlore oxides, *Rev. Mod. Phys.* **82**, 53 (2010).
- [19] J. G. Rau and M. J. P. Gingras, Frustrated quantum rare-earth pyrochlores, *Annu. Rev. Condens. Matter Phys.* **10**, 357 (2019).
- [20] S. T. Bramwell and M. J. P. Gingras, Spin ice state in frustrated magnetic pyrochlore materials, *Science* **294**, 1495 (2001).
- [21] C. Nisoli, R. Moessner, and P. Schiffer, Colloquium: Artificial spin ice: Designing and imaging magnetic frustration, *Rev. Mod. Phys.* **85**, 1473 (2013).
- [22] C. Castelnovo, R. Moessner, and S. L. Sondhi, Spin ice, fractionalization, and topological order, *Annu. Rev. Condens. Matter Phys.* **3**, 35 (2012).
- [23] S. H. Lee, H. Takagi, D. Louca, M. Matsuda, S. Ji, H. Ueda, Y. Ueda, T. Katsufuji, J. H. Chung, S. Park, S. W. Cheong, and C. Broholm, Frustrated magnetism and cooperative phase transitions in spinels, *J. Phys. Soc. Jpn.* **79**, 011004 (2010).
- [24] Y. Yafet and C. Kittel, Antiferromagnetic arrangements in ferrites, *Phys. Rev.* **87**, 290 (1952).
- [25] J. H. Lee, J. Ma, S. E. Hahn, H. B. Cao, M. Lee, T. Hong, H. J. Lee, M. S. Yeom, S. Okamoto, H. D. Zhou, M. Matsuda, and R. S. Fishman, Magnetic frustration driven by itinerancy in spinel CoV_2O_4 , *Sci. Rep.* **7**, 17129 (2017).
- [26] D. Reig-i Plessis, S. V. Geldern, A. A. Aczel, D. Kochkov, B. K. Clark, and G. J. MacDougall, Deviation from the dipole-ice model in the spinel spin-ice candidate MgEr_2Se_4 , *Phys. Rev. B* **99**, 134438 (2019).
- [27] N. Tristan, J. Hemberger, A. Krimmel, H. A. K. von Nidda, V. Tsurkan, and A. Loidl, Geometric frustration in the cubic spinels $M\text{Al}_2\text{O}_4$ ($M=\text{Co}$, Fe , and Mn), *Phys. Rev. B* **72**, 174404 (2005).
- [28] T. Suzuki, H. Nagai, M. Nohara, and H. Takagi, Melting of antiferromagnetic ordering in spinel oxide CoAl_2O_4 , *J. Phys.: Condens. Matter* **19**, 145265 (2007).
- [29] V. Fritsch, J. Hemberger, N. Buttgen, E. W. Scheidt, H. A. K. von Nidda, A. Loidl, and V. Tsurkan, Spin and Orbital Frustration in MnSc_2S_4 and FeSc_2S_4 , *Phys. Rev. Lett.* **92**, 116401 (2004).
- [30] J. R. Chamorro, L. Ge, J. Flynn, M. A. Subramanian, M. Mourigal, and T. M. McQueen, Frustrated spin one on a diamond lattice in NiRh_2O_4 , *Phys. Rev. Mater.* **2**, 034404 (2018).
- [31] X. R. Liu, S. Singh, B. J. Kirby, Z. C. Zhong, Y. W. Cao, B. Pal, M. Kareev, S. Middey, J. W. Freeland, P. Shafer, E. Arenholz, D. Vanderbilt, and J. Chakhalian, Emergent magnetic state in (111)-oriented quasi-two-dimensional spinel oxides, *Nano Lett.* **19**, 8381 (2019).
- [32] X. Liu, T. Asaba, Q. Zhang, Y. Cao, B. Pal, S. Middey, P. Kumar, M. Kareev, L. Gu, D. Sarma, P. Shafer, E. Arenholz, J. Freeland, L. Li, and J. Chakhalian, Quantum spin liquids by geometric lattice design, [arXiv:1911.00100](https://arxiv.org/abs/1911.00100).
- [33] S. E. Dutton, Q. Huang, O. Tchernyshyov, C. L. Broholm, and R. J. Cava, Sensitivity of the magnetic properties of the ZnCr_2O_4 and MgCr_2O_4 spinels to nonstoichiometry, *Phys. Rev. B* **83**, 064407 (2011).
- [34] L. Ortega-San-Martin, A. J. Williams, C. D. Gordon, S. Klemme, and J. P. Attfield, Low temperature neutron diffraction study of MgCr_2O_4 spinel, *J. Phys.: Condens. Matter* **20**, 104238 (2008).
- [35] D. W. McComb, A. J. Craven, L. Chioncel, A. I. Lichtenstein, and F. T. Docherty, Effect of short-range magnetic ordering on electron energy-loss spectra in spinels, *Phys. Rev. B* **68**, 224420 (2003).
- [36] M. T. Rovers, P. P. Kyriakou, H. A. Dabkowska, G. M. Luke, M. I. Larkin, and A. T. Savici, Muon-spin-relaxation investigation of the spin dynamics of geometrically frustrated chromium spinels, *Phys. Rev. B* **66**, 174434 (2002).
- [37] H. Suzuki and Y. Tsunoda, Spinel-type frustrated system MgCr_2O_4 studied by neutron scattering and magnetization measurements, *J. Phys. Chem. Solids* **68**, 2060 (2007).
- [38] M. C. Kemei, P. T. Barton, S. L. Moffitt, M. W. Gaultois, J. A. Kurzman, R. Seshadri, M. R. Suchomel, and Y. I. Kim, Crystal structures of spin-Jahn-Teller-ordered MgCr_2O_4 and ZnCr_2O_4 , *J. Phys.: Condens. Matter* **25**, 326001 (2013).
- [39] K. Tomiyasu, H. Suzuki, M. Toki, S. Itoh, M. Matsuura, N. Aso, and K. Yamada, Molecular Spin Resonance in the Geometrically Frustrated Magnet MgCr_2O_4 by Inelastic Neutron Scattering, *Phys. Rev. Lett.* **101**, 177401 (2008).
- [40] K. Tomiyasu, T. Yokobori, Y. Kousaka, R. I. Bewley, T. Guidi, T. Watanabe, J. Akimitsu, and K. Yamada, Emergence of Highly Degenerate Excited States in the Frustrated Magnet MgCr_2O_4 , *Phys. Rev. Lett.* **110**, 077205 (2013).

- [41] A. Miyata, H. Ueda, and S. Takeyama, Canted 2:1:1 magnetic supersolid phase in a frustrated magnet MgCr_2O_4 as a small limit of the biquadratic spin interaction, *J. Phys. Soc. Jpn.* **83**, 063702 (2014).
- [42] X. Bai, J. A. M. Paddison, E. Kapit, S. M. Koohpayeh, J. J. Wen, S. E. Dutton, A. T. Savici, A. I. Kolesnikov, G. E. Granroth, C. L. Broholm, J. T. Chalker, and M. Mourigal, Magnetic Excitations of the Classical Spin Liquid MgCr_2O_4 , *Phys. Rev. Lett.* **122**, 097201 (2019).
- [43] U. Luders, F. Sanchez, and J. Fontcuberta, Initial stages in the growth of 111-faceted CoCr_2O_4 clusters: Mechanisms and strained nanometric pyramids, *Appl. Phys. A* **79**, 93 (2004).
- [44] J. Chakhalian, X. R. Liu, and G. A. Fiete, Strongly correlated and topological states in 111 grown transition metal oxide thin films and heterostructures, *APL Mater.* **8**, 050904 (2020).
- [45] X. R. Liu, S. Middey, Y. W. Cao, M. Kareev, and J. Chakhalian, Geometrical lattice engineering of complex oxide heterostructures: A designer approach to emergent quantum states, *MRS Commun.* **6**, 133 (2016).
- [46] N. W. Grimes, Structural distortions in MgCr_2O_4 , *J. Phys. C: Solid State Phys.* **4**, L342 (1971).
- [47] N. F. Kosenko, N. V. Filatova, and A. A. Egorova, Magnesiochromite (MgCr_2O_4) synthesis: Effect of mechanical and microwave pretreatment, *Izv. Vyssh. Uchebn. Zaved., Khim. Khim. Tekhnol.* **63**, 96 (2020).
- [48] J. N. Hu, W. Y. Zhao, R. S. Hu, G. Y. Chang, C. Li, and L. J. Wang, Catalytic activity of spinel oxides MgCr_2O_4 and CoCr_2O_4 for methane combustion, *Mater. Res. Bull.* **57**, 268 (2014).
- [49] E. Jafarnejad, S. Khanahmadzadeh, F. Ghanbary, and M. Enhessari, Synthesis, characterization and optical band gap of pirochromite (MgCr_2O_4) nanoparticles by stearic acid sol-gel method, *Curr. Chem. Lett.* **5**, 173 (2016).
- [50] S. M. Koohpayeh, J. J. Wen, M. Mourigal, S. E. Dutton, R. J. Cava, C. L. Broholm, and T. M. McQueen, Optical floating zone crystal growth and magnetic properties of MgCr_2O_4 , *J. Cryst. Growth* **384**, 39 (2013).
- [51] S. K. Durrani, S. Naz, M. Nadeem, and A. A. Khan, Thermal, structural, and impedance analysis of nanocrystalline magnesium chromite spinel synthesized via hydrothermal process, *J. Therm. Anal. Calorim.* **116**, 309 (2014).
- [52] L. V. Morozova and V. P. Popov, Synthesis and investigation of magnesium chromium spinel, *Glass Phys. Chem.* **36**, 86 (2010).
- [53] L. Bindi, E. Sirotkina, A. V. Bobrov, and T. Irifune, X-ray single-crystal structural characterization of mgcr_2o_4 , a post-spinel phase synthesized at 23 GPa and 1600 °C, *J. Phys. Chem. Solids.* **75**, 638 (2014).
- [54] M. K. Rasmussen, K. Meinander, F. Besenbacher, and J. V. Lauritsen, Noncontact atomic force microscopy study of the spinel $\text{MgAl}_2\text{O}_4(111)$ surface, *Beilstein J. Nanotechnol.* **3**, 192 (2012).
- [55] N. Daneu, A. Recnik, T. Yamazaki, and T. Dolenc, Structure and chemistry of (111) twin boundaries in MgAl_2O_4 spinel crystals from Mogok, *Phys. Chem. Miner.* **34**, 233 (2007).
- [56] H. J. Noh, J. Jeong, B. Chang, D. Jeong, H. S. Moon, E. J. Cho, J. M. Ok, J. S. Kim, K. Kim, B. I. Min, H. K. Lee, J. Y. Kim, B. G. Park, H. D. Kim, and S. Lee, Direct observation of localized spin antiferromagnetic transition in PdCrO_2 by angle-resolved photoemission spectroscopy, *Sci. Rep.* **4**, 3680 (2014).
- [57] M. C. Biesinger, C. Brown, J. R. Mycroft, R. D. Davidson, and N. S. McIntyre, X-ray photoelectron spectroscopy studies of chromium compounds, *Surf. Interface Anal.* **36**, 1550 (2004).
- [58] B. P. Payne, M. C. Biesinger, and N. S. McIntyre, X-ray photoelectron spectroscopy studies of reactions on chromium metal and chromium oxide surfaces, *J. Electron Spectrosc. Relat. Phenom.* **184**, 29 (2011).
- [59] A. R. Kaul, O. Y. Gorbenco, and A. A. Kamenev, The role of heteroepitaxy in the development of new thin-film oxide-based functional materials, *Usp. Khim.* **73**, 932 (2004).
- [60] K. T. Jacob, Potentiometric determination of the Gibbs free energy of formation of cadmium and magnesium chromites, *J. Electrochem. Soc.* **124**, 1827 (1977).
- [61] R. K. Mishra and G. Thomas, Surface-energy of spinel, *J. Appl. Phys.* **48**, 4576 (1977).
- [62] T. Watanabe, S. Ishikawa, H. Suzuki, Y. Kousaka, and K. Tomiyasu, Observation of elastic anomalies driven by co-existing dynamical spin Jahn-Teller effect and dynamical molecular-spin state in the paramagnetic phase of frustrated MgCr_2O_4 , *Phys. Rev. B* **86**, 144413 (2012).
- [63] S. Lal and S. K. Pandey, The role of ionic sizes in inducing the cubic to tetragonal distortion in AV_2O_4 and ACr_2O_4 ($A = \text{Zn, Mg and Cd}$) compounds, *Mater. Res. Express* **3**, 116301 (2016).